nanomaterials

MDPI

Article

An Investigation on the Synthesis of Molybdenum Oxide and Its Silica Nanoparticle Composites for Dye Degradation

Olfa Kamoun [1], Abdelaziz Gassoumi [2,*], Salah Kouass [3], Badriyah Alhalaili [4], Ruxandra Vidu [5,6,*] and Najoua Turki-Kamoun [1]

1 Laboratoire de Physique de la Matière Condensée, Faculté des Sciences de Tunis, Université de Tunis El Manar, Tunis 2092, Tunisia; o.kamoun@yahoo.fr (O.K.); n.najouakamoun@gmail.com (N.T.-K.)
2 Department of Physics, Faculty of Science, King Khalid University, P.O. Box 9004, Abha 61413, Saudi Arabia
3 Laboratoire Matériaux Utiles, Institut National de Recherche et d'Analyse Physico-Chimique (INRAP) Sidi Thabet, Ariana 2020, Tunisia; kouasssa@gmail.com
4 Nanotechnology and Advanced Materials Program, Kuwait Institute for Scientific Research, P.O. Box 24885, Safat 13109, Kuwait; bhalaili@kisr.edu.kw
5 Department of Electrical and Computer Engineering, University of California Davis, Davis, CA 95616, USA
6 Faculty of Materials Science and Engineering, University POLITEHNICA of Bucharest, 313 Splaiul Independentei, RO-060042 Bucharest, Romania
* Correspondence: abdelaziz.gassoumi@gmail.com (A.G.); rvidu@ucdavis.edu (R.V.)

Received: 6 November 2020; Accepted: 29 November 2020; Published: 2 December 2020

Abstract: The molybdenum oxide (MoO_3) and MoO_3@SiO_2 nanoparticles were successfully prepared using the chemical bath deposition (CBD) method. The photocatalytic activities of molybdenum oxide (MoO_3), SiO_2, and MoO_3@SiO_2 nanoparticles composite have shown a synergistic photocatalytic effect of SiO_2 combined with MoO_3. The first-order degradation rate constants for MoO_3, SiO_2, and MoO_3@SiO_2 nanocomposite were 10.3×10^{-3} min^{-1}, 15.1×10^{-3} min^{-1}, and 16.3×10^{-3} min^{-1}, respectively. The MoO_3@SiO_2 composite showed degradation efficiencies in the methylene blue solution close to 100% after 60 min of UV irradiation. The X-ray diffraction (XRD) showed that the MoO_3 powder has a hexagonal crystal structure and the silica is the tridymite type of SiO_2. The crystallite size was about 94 nm, 32 nm, and 125 nm for MoO_3, silica, and MoO_3@SiO_2, respectively, as calculated by the Scherrer equation. The scanning electron microscopy (SEM) images revealed that the MoO_3 powder consisted of a uniform hexagonal structure; the silica showed a rod-like micro-flake morphology and the MoO_3@SiO_2 composite had the appearance of coral-like structures.

Keywords: MoO_3 nanoparticles; silica; nanoparticle composite; structural properties; photocatalytic properties; methylene blue

1. Introduction

Catalytic materials were developed over the years to purify the polluted water and air, where the heterogeneous photocatalysis plays an important role [1–5]. The well-known transition metal oxide photocatalysts are ZnO [6], TiO_2 [7], WO_3 [8], and MoO_3 [9]. The oxidation process of heterogeneous photocatalysis is achieved by using light to activate the catalyst and to generate highly reactive free radicals, which then reduce particular organic compounds [6,7,9–11]. When the mineralization process is finished, the outcome consists of H_2O and CO_2.

The photocatalytic mechanism is activated when the oxide semiconductor is immersed in a liquid or placed in a gaseous medium and then irradiated with light of an energy that is equal to or greater

than its bandgap [11]. In this case, electron-hole pairs are generated on the surface of the semiconductor and subsequent chemical reactions with the environmental media lead to the production of free radicals, which degrade the organic pollutants [10,11].

Photocatalysis requires a large surface area for reaction. The exterior of natural silica is covered with a network of pores to optimize the capture of light. This feature of silica has attracted the attention of nanotechnologists. Moreover, silica is a phylum of unicellular microalgae (from 2 µm to 1 mm) present in all aquatic environments, and the majorities are in biofilms (with a preference for cold water) and enveloped by a siliceous external skeleton. The degradation of MB under the visible light has been demonstrated for photocatalysts prepared using green and renewable resources [12]. Mesoporous silica impregnated with Pt-Porphyrin or PtNPs [13] and titania sensitized with porphyrin [14] or magnetic photocatalyst porphyrin [15] has also been shown visible-light-driven photocatalysis. MoO_3 is one of the most promising metal oxides because of its many advantages, such as its non-toxic nature, and can be widely used in an organic light-emitting diode, gas sensing, catalysis, transistors, and solar cells [16–18]. The smaller the particle size of MoO_3, the larger the surface area, which potentially increases the adsorption methylene blue and photoactive sites, resulting in enhanced photocatalytic activity [9,16,19]. Various methods have been used to optimize the preparation and processing technology of molybdenum oxide films, such as thermal evaporation, sol–gel deposition, and chemical vapor deposition [20–22]. In our work, we used a simple and inexpensive chemical bath deposition (CBD) technique because the film properties can be optimized through various deposition process parameters. The CBD technique has received great consideration from the research community for the production of low-cost semiconductor photocatalyst.

In our search for novel and sustainable photocatalysts, we used the unique architecture of silica and high surface area to increase the degradation efficiency of the organic dyes. Because MoO_3 has shown good photocatalytic degradation properties [23–25], present in this study the synthesis of a novel MoO_3 and SiO_2 nanoparticle composites, labeled MoO_3@SiO_2, and their photocatalytic properties. The main objective of this work is to study the photocatalytic activities of the films for the photodegradation of methylene blue (MB) under UV light, as well as examine the physical properties of the MoO_3 films.

2. Experimental and Characterization Details

The chemical bath deposition (CBD) method was performed to synthesize nanocrystalline MoO_3 and MoO_3 on SiO_2, as illustrated in Figure 1. In a typical synthesis, an aqueous solution of 15 mL of 0.05 M $(NH_4)_6Mo_7O_{24}{\cdot}4H_2O$ (99%, Merck, Kenilworth, NJ, USA) solution was mixed with SiO_2 in a reaction bath. The temperature of the reaction bath was slowly increased to 50 °C. Then, 5 mL of concentrated HNO_3 (ACS reagent, ≥90.0%) was added dropwise with constant stirring until the pH of the solution was 2.2, and a clear solution was obtained. Then, after the solution was stirred for 15 min, the temperature of the reaction bath was raised to 70 °C, where the initial seeds started to form. The reaction bath was held at 70 °C for 30 min, during which time a white precipitate of h-MoO_3 nanoparticles was observed. When the synthesis was complete, the white precipitate was filtered using deionized water and then dried in an oven at a constant temperature of 110 °C for 1 h [26,27].

The nanoparticle composites were analyzed by X-ray diffraction (XRD) scanning electron microscopy (SEM), and UV-Vis spectroscopy. The XRD patterns were recorded on an X'pert PRO X-ray diffractometer (Malvern Panalytical Ltd, Malvern, UK) with graphite monochromatized Cu Kα radiation source (1.5406 Å). Morphologies of nanopowders were examined using a JEOL-JSM-6490 LV scanning electron microscope (SEMTech Solutions, Inc., North Billerica, MA, USA) and absorbance measurements were performed using a Perkin Elmer Lambda 950 spectrometer (Perkin Elmer, Waltham, MA, USA). The UV irradiation was performed at 254 nm wavelength using an 8 W power lamp (Philips Germicidal Ultraviolet-C, Philips Lightning, Eindhoven, The Netherlands).

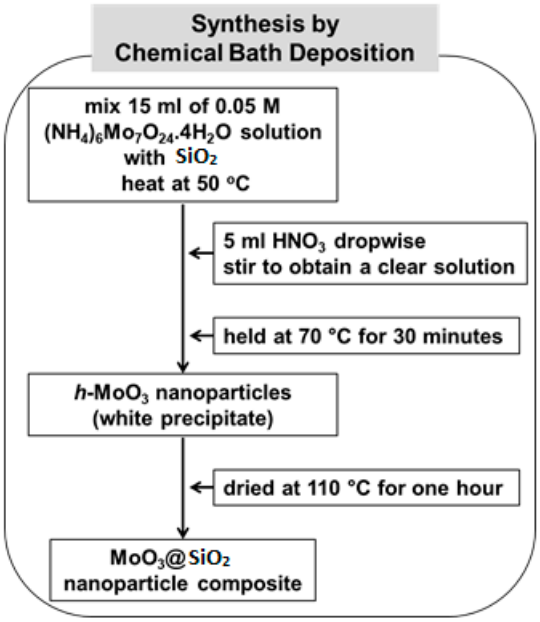

Figure 1. Illustration of the processing steps in the synthesis of MoO_3@SiO_2 nanoparticle composites.

3. Results and Discussion

3.1. Structural Properties

Both MoO_3 nanoparticles and SiO_2 were analyzed by X-ray diffraction analysis and compared to the MoO_3@SiO_2 nanoparticles composite. Figure 2 shows the XRD patterns of the MoO_3, SiO_2, and MoO_3@SiO_2 nanoparticles grown by chemical bath deposition. The diffraction patterns correspond to the h-MoO_3 phase for the MoO_3 nanoparticles and to tridymite, which is the monoclinic phase corresponding to SiO_2 for the silica [28].

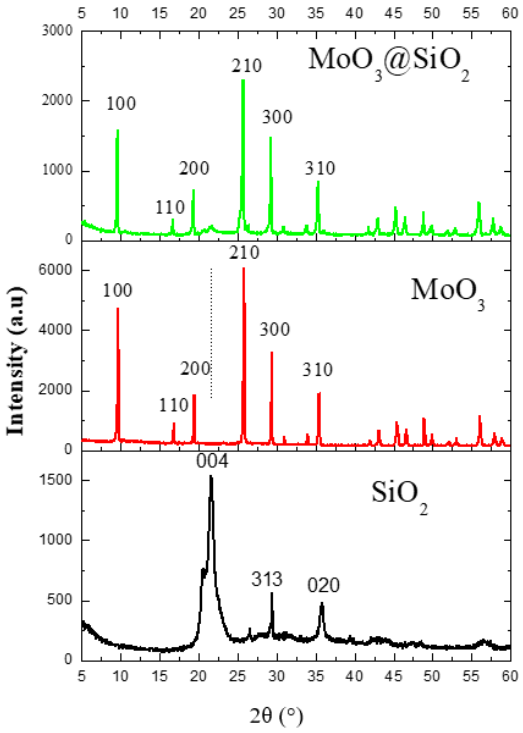

Figure 2. The XRD patterns for the SiO_2, MoO_3, and the MoO_3@SiO_2 composite.

Tridymite is a species of mineral of the tectosilicate family, and one of the polymorphs of silica with quartz, coesite, cristobalite, stishovite, having the chemical formula of SiO_2 and containing traces of titanium, aluminum, iron, manganese, magnesium, calcium, sodium, and potassium.

MoO_3 has the following lattice parameters: a = 10.53 Å and c = 14.876 Å (JCPDS card no. 21-0569) [19]. The SiO_2 has the following lattice parameters: a = 25.93 Å, b = 5.01 Å, and c = 18.54 Å, with the highest intensity at 2θ = 21.6°, matching the reference R090042 [29].

The crystallite size can be estimated from the full width half maximum (FWHM) values obtained from the predominant (210) for MoO_3 and MoO_3@SiO_2 diffraction peak at 2θ = 25.7° according to the following Debye–Sherrer equation [30–32]:

$$D = 0.9\lambda/\beta\cos\theta \quad (1)$$

where λ is the wavelength of Cu-Kα1 radiation (1.5406 Å) and θ is the Bragg diffraction angle. The crystallite sizes calculated with Equation (1) were around 94, 32, and 125 nm for MoO_3, SiO_2, and MoO_3@SiO_2, respectively. The observed broadening of the SiO_2 peak(004) in the MoO_3@SiO_2 spectrum is attributed to the size and strain effect between MoO_3 and SiO_2 [19].

In the XRD spectra of the MoO_3@SiO_2 composite, all peaks attributed to the MoO_3phase are observed, which confirms that the MoO_3 nanoparticles are well grown on the SiO_2 surface. It was also observed that the intensity for all MoO_3 peaks decreases for MoO_3@SiO_2 composite compared to those of MoO_3. Note the existence of the preferential SiO_2 peak at 2θ = 21.6°. All MoO_3@SiO_2 peaks decreased in intensity, which may be due to the fact that MoO_3 nanoparticles are well-formed on the surface of SiO_2, but in a dispersed manner.

3.2. Morphological Analysis

Surface morphology of the nanoparticles composite and constituent nanoparticles were investigated by using SEM analyses. The nanoparticles of MoO_3 consist of a uniform hexagonal rod-like morphology. The regular faceted surface of each hexagonal rod [33] is clearly seen in Figure 3a. In Figure 3b, stems have developed out of a central point [34], with flower-like clusters of hexagonal MoO_3 stem-shaped petals. The SEM images of SiO_2 (Figure 3c) shows a similar morphology as SiO_2 [35]. The morphology of SiO_2 depicts mostly micro-flake and irregular rod-shaped with particles agglomeration. Regarding the MoO_3@SiO_2 composite (Figure 3d,e), we observed the appearance of coral-like structures in the form of hexagonal rods. The morphology of this composite indicates the incorporation of MoO_3 into the SiO_2 in the MoO_3@SiO_2 composite, which is in agreement with the XRD analysis in Figure 2. SEM observation shows that the specific surface area increased for the MoO_3@SiO_2 composite compared to those for MoO_3 or SiO_2. Increasing the specific surface area, especially in the case of MoO_3@SiO_2, could play an important role in improving sensitivity in optoelectronic applications like photocatalysis and gas sensors.

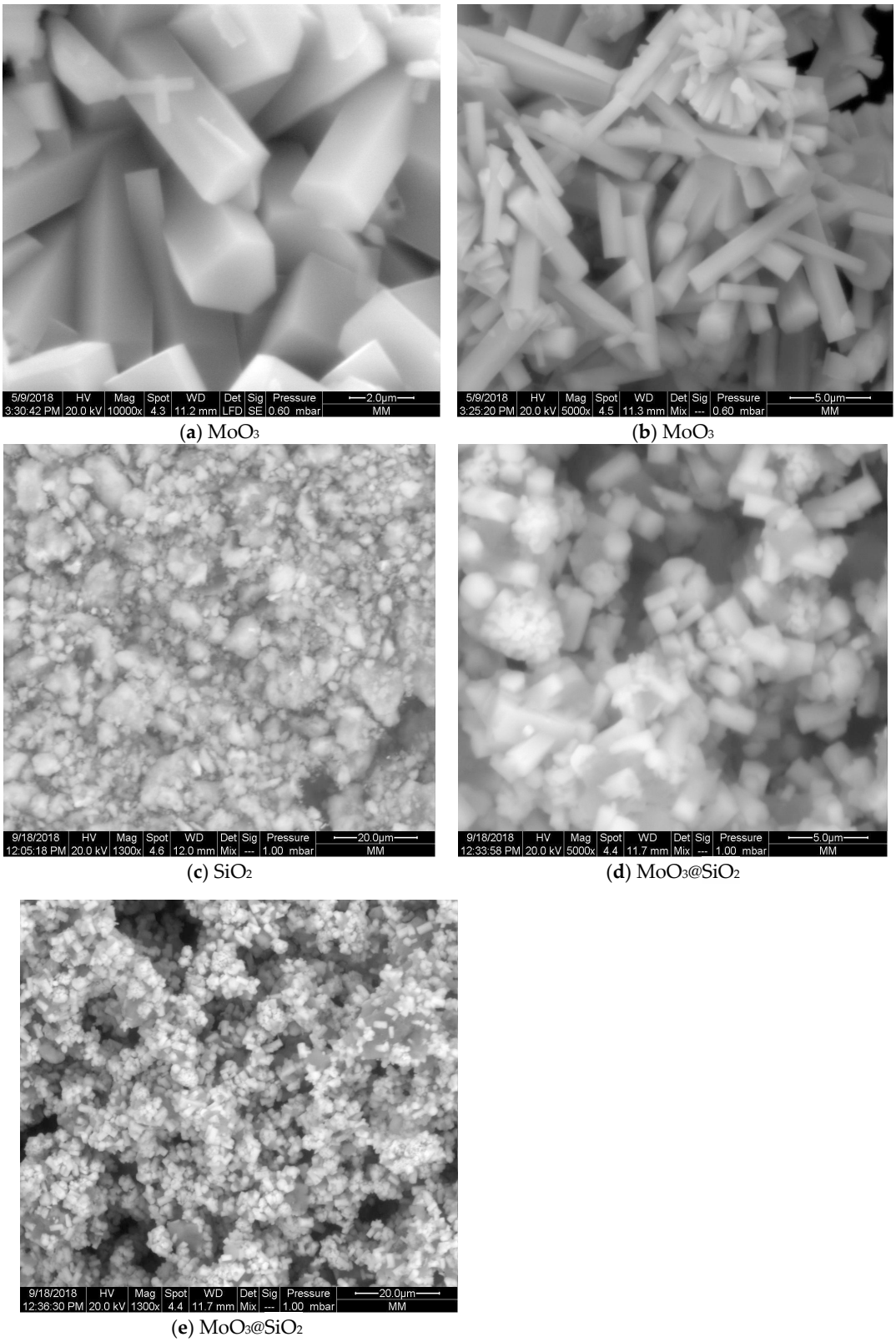

(**a**) MoO_3 (**b**) MoO_3

(**c**) SiO_2 (**d**) MoO_3@SiO_2

(**e**) MoO_3@SiO_2

Figure 3. SEM micrographs of MoO_3nanoparticles (**a**,**b**), silica particles (**c**), and MoO_3@SiO_2 nanoparticles composites (**d**,**e**) at different magnifications.

3.3. Photocatalytic Studies

MoO_3 nanoparticles were used as photocatalyst for the degradation of methylene blue (MB), which was used as a model compound. It was found that there was no MB degradation in the dark and in the presence of MoO_3, SiO_2, and MoO_3@SiO_2. In this work, we have monitored the MB degradation under UV light at different times with MoO_3, SiO_2, and MoO_3@SiO_2 nanoparticle catalysts. Figure 4 presents the UV-Vis absorption spectra of MoO_3 nanoparticles, SiO_2 and MoO_3@SiO_2 nanoparticles exposed to UV light for different times.

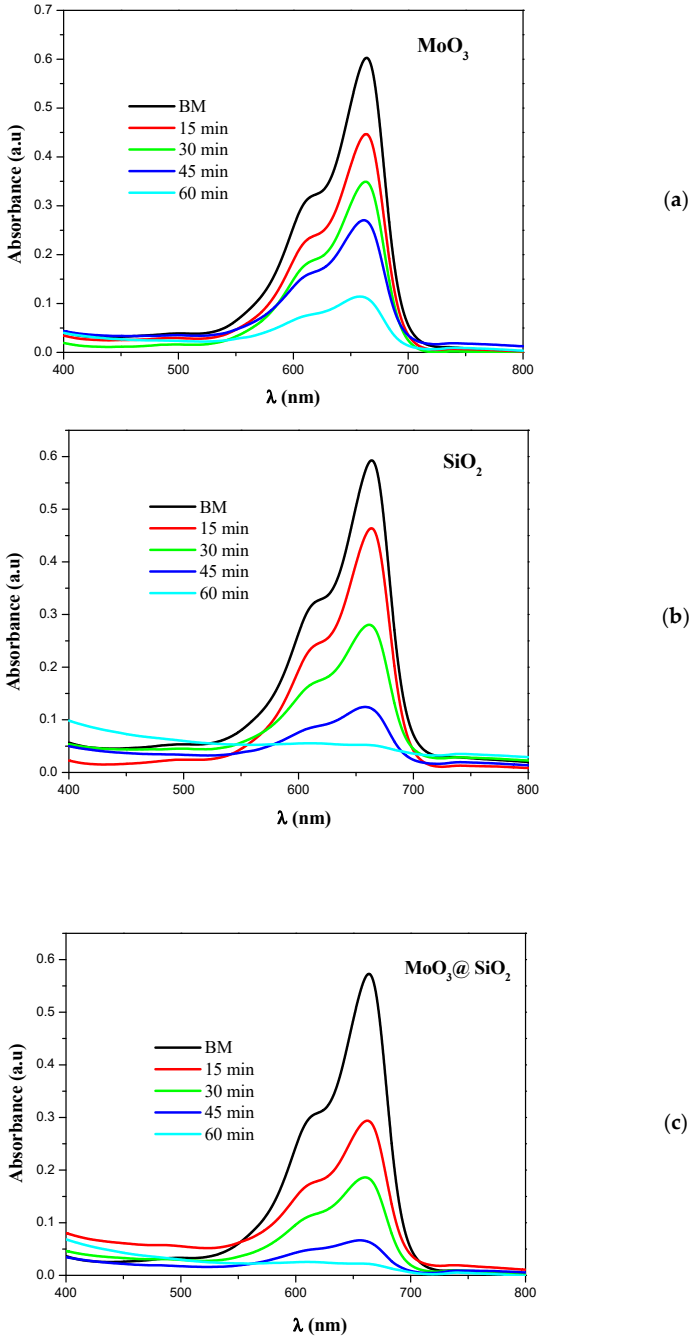

Figure 4. UV-Vis absorption spectra of MoO_3 nanoparticles (**a**), SiO_2 (**b**) and MoO_3@SiO_2 (**c**).

There are two different absorption bands for the aqueous cationic MB dye solution, i.e., at 293 nm (π-π*) and 664 nm (n-π*) [34]. In this work, the intensities of the absorption peaks at 664 nm decrease

with increasing the time of irradiation, compared to the catalyst-free solution. The degradation of the MB solution containing h-MoO_3 catalyst synthesized by CBD was 90% [34].

During photocatalysis, the electrons in the valence band of the oxide semiconductor are excited under UV light radiation and leave holes in the valence band after they jump to the conduction band. The holes combine with H_2O to produce · H and · OH radicals. In the meanwhile, the electrons in the conduction band scattered towards the adsorbed O_2 to generate activated · O_2 [36] with the consequent transformation of the water molecules into · OH radicals.

The mechanism of photocatalytic degradation for MoO_3nanoparticles is similar to that of a metal oxide semiconductor [37], as follows:

$$MoO_3 \text{ (or } SiO_2 \text{ or composite)} + h\nu \rightarrow MoO_3\ (e^- + h^+) \quad (2)$$

$$h^+ + OH^- \rightarrow OH^{\cdot} \text{ (hydroxide)} \quad (3)$$

$$e^- + O_2 \rightarrow O_2^- \text{ (super oxide anion)} \quad (4)$$

$$OH^{\cdot} + MB \rightarrow MB^* \text{ (intermediate)} \rightarrow CO_2 + H_2O \quad (5)$$

$$O_2^- + MB \rightarrow MB^* \text{ (intermediate)} \rightarrow CO_2 + H_2O \quad (6)$$

These oxidizing species can degrade the MB dye into chemical forms of CO_2 and H_2O, which is a better solution to water remediation treatments [36]. If the photocatalytic processes do not take place, the recombination of the (e^- + h^+) pairs happens, and heat is generated in the materials. The photocatalytic activity depends on various factors, including the structure and the dimension of the particles, degree of crystallinity, specific surface area, adsorbed water molecules, and hydroxyl groups [38–41].

The degradation efficiency was further studied in the presence of h-MoO_3, SiO_2, and MoO_3@SiO_2 nanoparticle composite in MB dye, and the results are presented in Figure 5. The degradation efficiency was calculated using the following equation [42,43]:

$$\textit{Degradation efficiency} = (C_0 - C)/C_0\ (\%) \quad (7)$$

where C_0 is the initial dye concentration in the solution, and C is the dye concentration in the solution after irradiation, for a given time interval [42].

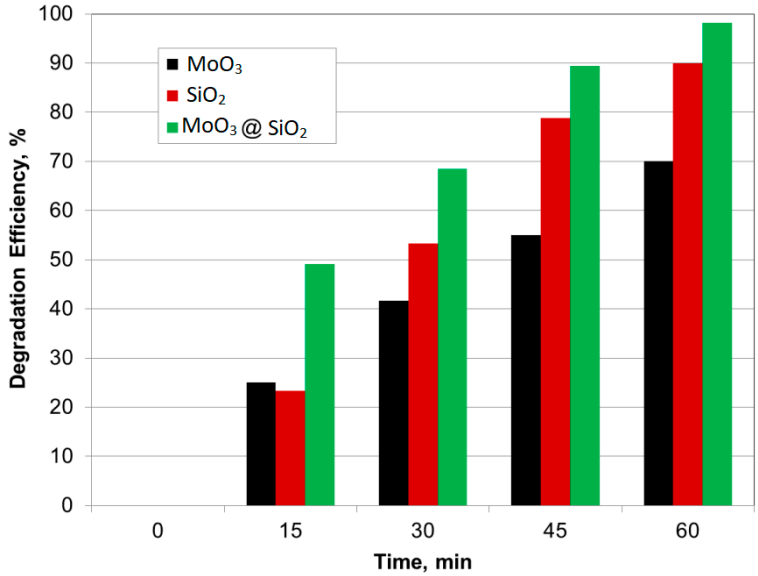

Figure 5. Comparative bar diagram of degradation efficiency for MoO_3, SiO_2, and MoO_3@SiO_2.

Figure 5 shows that the degradation efficiency increases with exposure time under UV-light. The MoO_3@SiO_2 composite showed degradation efficiencies in the MB solution close to 100% after 60 min of UV irradiation. The MoO_3@SiO_2 composite showed stable rates of MB photodegradation up to six cycles.

The rate kinetics analysis, an important parameter in the degradation studies, was performed to predict the rate at which MB is removed from the aqueous solution [42]. In these experiments, different amounts of MoO_3, SiO_2, and MoO_3@SiO_2 composite were used with a fixed concentration of MB. The reaction kinetics was calculated with Equation (8) [42]:

$$Ln(C/C_0) = -kt \quad (8)$$

where C_0 and C were defined for Equation (7). The graph of the natural logarithm, $Ln(C/C_0)$ for MB dye versus time in the presence of MoO_3, SiO_2, and MoO_3@SiO_2 nanocomposite is presented in Figure 6.

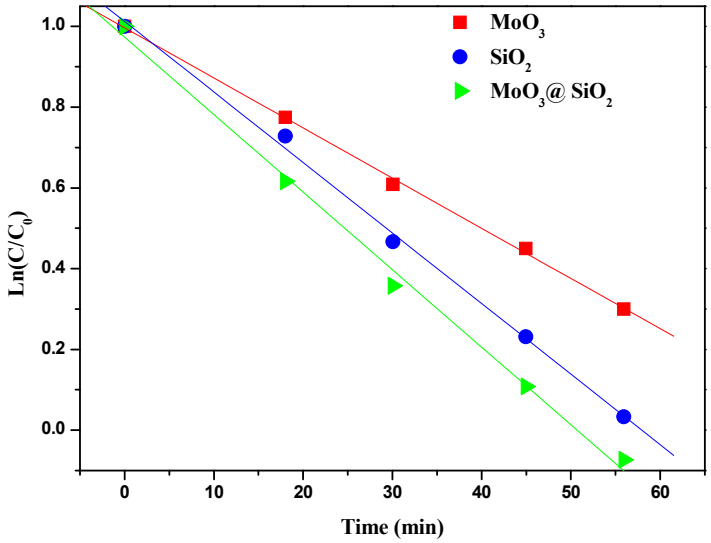

Figure 6. The plots of $Ln(C/C_0)$ versus time for MoO_3, SiO_2, and MoO_3@SiO_2.

The MB concentration presented in log scale in Figure 6 varies practically linearly with time, indicating that the photodegradation of MB dye follows the first-order kinetics [42]. The kinetic rate constants (k) were determined from the slope of fitted curves. The first-order degradation rate constants for MoO_3, SiO_2, and MoO_3@SiO_2 nanocomposite were 10.3×10^{-3} min^{-1}, 15.1×10^{-3} min^{-1}, and 16.3×10^{-3} min^{-1}, respectively. Table 1 presents the rate constants for MB degradation obtained in this work in comparison to other literature data. The degradation rate of MB is faster for MoO_3@SiO_2 nanocomposite compared to MoO_3 or SiO_2.

Table 1. Comparative rate constants for different photocatalysts, including our work.

Material	Rate Constants $\times 10^{-3}$ min^{-1}	References
MoO_3 (CBD)	10.3	this work
SiO_2	15.1	this work
MoO_3@SiO_2	16.3	this work
MoO_3	0.334	[44]
ZnO	15.15	[6]
α-Fe_2O_3	2.01	[45]
SnS_2	4.43	[45]
$SrFe_{12}O_{19}$	13.6	[46]
TiO_2	35.58	[47]

4. Conclusions

We have synthesized MoO_3@SiO_2 nanoparticle composite using chemical bath deposition. The diffraction patterns are in good agreement with the hexagonal phase MoO_3 with the lattice parameters of a = 10.53 Å and c = 14.876 Å. The SiO_2 has the following lattice parameters: a = 25.93 Å, b = 5.01 Å, and c = 18.54 Å. The XRD analysis showed that MoO_3, silica, and MoO_3@SiO_2 nanoparticle composite have crystalline characteristics phase with an average crystallite size of about 94 nm, 32 nm, and 125 nm, respectively. SiO_2 showed micro-flakes morphology with agglomeration as confirmed by SEM analysis, irregular rod-shaped for MoO_3, and coral-like structure for MoO_3@SiO_2. The optimum photocatalytic activity was found for MoO_3@SiO_2 nanoparticles, with an efficiency of about 100% after 60 min of exposure to the UV-light, while the degradation efficiency for the same UV exposure time was about 90% and 70% for SiO_2 and MoO_3, respectively. The degradation rate constants for MoO_3, SiO_2, and MoO_3@SiO_2 nanocomposite were 10.3×10^{-3} min^{-1}, 15.1×10^{-3} min^{-1}, and 16.3×10^{-3} min^{-1}, respectively. These results show that SiO_2 particles have a beneficial photocatalytic effect combined with MoO_3 in the MoO_3@SiO_2 composite in the photocatalytic processes.

Author Contributions: Conceptualization: O.K. and A.G.; methodology, O.K. and A.G.; validation, O.K. and A.G.; formal analysis, O.K., B.A., and A.G.; investigation: S.K. and B.A.; resources: A.G. and N.T.-K.; writing—original draft preparation, O.K. and A.G.; writing—review and editing, O.K., A.G., B.A., and R.V.; visualization, O.K., B.A., and A.G.; supervision, N.T.-K. and R.V.; project administration, A.G. and O.K.; funding acquisition, A.G. and N.T.-K. All authors have read and agreed to the published version of the manuscript.

Funding: This research was funded by the Deanship of Scientific Research- Research Center at King Khalid University in Saudi Arabia, code number: GRP-95-41. This project is carried out under the mobility (MOBI) for doctoral and post-doctoral students (DOC) (MOBIDOC) scheme, funded by the European Union (EU) through the Education, Mobility, Research and Innovation (EMORI) program and managed by the National Agency for the Promotion of Scientific Research (ANPR).

Conflicts of Interest: The authors declare no conflict of interest.

References

1. Bolisetty, S.; Peydayesh, M.; Mezzenga, R. Sustainable technologies for water purification from heavy metals: Review and analysis. *Chem. Soc. Rev.* **2019**, *48*, 463–487. [CrossRef]
2. DeCoste, J.B.; Peterson, G.W. Metal–organic frameworks for air purification of toxic chemicals. *Chem. Rev.* **2014**, *114*, 5695–5727. [CrossRef]
3. Pichat, P.; Disdier, J.; Hoang-Van, C.; Mas, D.; Goutailler, G.; Gaysse, C. Purification/deodorization of indoor air and gaseous effluents by TiO_2 photocatalysis. *Catal. Today* **2000**, *63*, 363–369. [CrossRef]
4. Shen, G.; Pan, L.; Zhang, R.; Sun, S.; Hou, F.; Zhang, X.; Zou, J.-J. Low-spin-state hematite with superior adsorption of anionic contaminations for water purification. *Adv. Mater.* **2020**, *32*, 1905988. [CrossRef]
5. Zhao, J.; Yang, X. Photocatalytic oxidation for indoor air purification: A literature review. *Build. Environ.* **2003**, *38*, 645–654. [CrossRef]
6. Bhatia, S.; Verma, N. Photocatalytic activity of zno nanoparticles with optimization of defects. *Mater. Res. Bull.* **2017**, *95*, 468–476. [CrossRef]
7. Li, H.; Wang, P.; Yi, X.; Yu, H. Edge-selectively amidated graphene for boosting h_2-evolution activity of TiO_2 photocatalyst. *Appl. Catal. B Environ.* **2020**, *264*, 118504. [CrossRef]
8. Nandiyanto, A.B.D.; Zaen, R.; Oktiani, R. Correlation between crystallite size and photocatalytic performance of micrometer-sized monoclinic WO_3 particles. *Arab. J. Chem.* **2020**, *13*, 1283–1296. [CrossRef]
9. Peña-Bahamonde, J.; Wu, C.; Fanourakis, S.K.; Louie, S.M.; Bao, J.; Rodrigues, D.F. Oxidation state of Mo affects dissolution and visible-light photocatalytic activity of MoO_3 nanostructures. *J. Catal.* **2020**, *381*, 508–519. [CrossRef]
10. Mimouni, R.; Souissi, A.; Madouri, A.; Boubaker, K.; Amlouk, M. High photocatalytic efficiency and stability of chromium-indium codoped ZnO thin films under sunlight irradiation for water purification development purposes. *Curr. Appl. Phys.* **2017**, *17*, 1058–1065. [CrossRef]

11. Ponce-Mosso, M.; Pérez-González, M.; García-Tinoco, P.E.; Crotte-Ledesma, H.; Morales-Luna, M.; Tomás, S.A. Enhanced photocatalytic activity of amorphous MoO_3 thin films deposited by rf reactive magnetron sputtering. *Catal. Today* **2020**, *349*, 150–158. [CrossRef]
12. Das, G.S.; Shim, J.P.; Bhatnagar, A.; Tripathi, K.M.; Kim, T. Biomass-derived carbon quantum dots for visible-light-induced photocatalysis and label-free detection of Fe(iii) and ascorbic acid. *Sci. Rep.* **2019**, *9*, 15084. [CrossRef]
13. Anghel, D.; Lascu, A.; Epuran, C.; Fratilescu, I.; Ianasi, C.; Birdeanu, M.; Fagadar-Cosma, E. Hybrid materials based on silica matrices impregnated with pt-porphyrin or ptnps destined for CO_2 gas detection or for wastewaters color removal. *Int. J. Mol. Sci.* **2020**, *21*, 4262. [CrossRef]
14. Wan, J.M.; Wu, Z.Z.; Wang, H.G.; Zheng, X.M. Visible-light photocatalytic degradation of methylene blue with porphyrin-sensitized TiO_2. *Adv. Mater. Res.* **2012**, *441*, 544–548. [CrossRef]
15. Gholamrezapor, E.; Eslami, A. Sensitization of magnetic TiO_2 with copper(ii) tetrahydroxylphenyl porphyrin for photodegradation of methylene blue by visible led light. *J. Mater. Sci. Mater. Electron.* **2019**, *30*, 4705–4715. [CrossRef]
16. Fernandes, C.I.; Capelli, S.C.; Vaz, P.D.; Nunes, C.D. Highly selective and recyclable MoO_3 nanoparticles in epoxidation catalysis. *Appl. Catal. A Gen.* **2015**, *504*, 344–350. [CrossRef]
17. Hanmandlu, C.; Chen, C.-Y.; Boopathi, K.M.; Lin, H.-W.; Lai, C.-S.; Chu, C.-W. Bifacial perovskite solar cells featuring semitransparent electrodes. *ACS Appl. Mater. Interfaces* **2017**, *9*, 32635–32642. [CrossRef]
18. Schulz, P.; Tiepelt, J.O.; Christians, J.A.; Levine, I.; Edri, E.; Sanehira, E.M.; Hodes, G.; Cahen, D.; Kahn, A. High-work-function molybdenum oxide hole extraction contacts in hybrid organic–inorganic perovskite solar cells. *ACS Appl. Mater. Interfaces* **2016**, *8*, 31491–31499. [CrossRef]
19. Manivel, A.; Lee, G.-J.; Chen, C.-Y.; Chen, J.-H.; Ma, S.-H.; Horng, T.-L.; Wu, J.J. Synthesis of MoO_3 nanoparticles for azo dye degradation by catalytic ozonation. *Mater. Res. Bull.* **2015**, *62*, 184–191. [CrossRef]
20. Lee, Y.J.; Nichols, W.T.; Kim, D.-G.; Kim, Y.D. Chemical vapour transport synthesis and optical characterization of MoO_3 thin films. *J. Phys. D Appl. Phys.* **2009**, *42*, 115419. [CrossRef]
21. Liu, F.; Shao, S.; Guo, X.; Zhao, Y.; Xie, Z. Efficient polymer photovoltaic cells using solution-processed MoO_3 as anode buffer layer. *Sol. Energy Mater. Sol. Cells* **2010**, *94*, 842–845. [CrossRef]
22. Navas, I.; Vinodkumar, R.; Lethy, K.J.; Detty, A.P.; Ganesan, V.; Sathe, V.; Mahadevan Pillai, V.P. Growth and characterization of molybdenum oxide nanorods by rf magnetron sputtering and subsequent annealing. *J. Phys. D Appl. Phys.* **2009**, *42*, 175305. [CrossRef]
23. Kamoun, O.; Boukhachem, A.; Alleg, S.; Jeyadevan, B.; Amlouk, M. Physical study of nano-structured MoO_3 films codoped with cobalt and nickel in which there is a ferro-diamagnetic transition. *J. Alloys Compd.* **2018**, *741*, 847–854. [CrossRef]
24. Kamoun, O.; Boukhachem, A.; Amlouk, M.; Ammar, S. Physical study of Eu doped MoO_3 thin films. *J. Alloys Compd.* **2016**, *687*, 595–603. [CrossRef]
25. Kamoun, O.; Mami, A.; Amara, M.A.; Vidu, R.; Amlouk, M. Nanostructured Fe,Co-codoped MoO_3 thin films. *Micromachines* **2019**, *10*, 138. [CrossRef]
26. Desai, N.; Mali, S. Chemically grown MoO_3 nanorods for antibacterial activity study. *J. Nanomed. Nanotechnol.* **2015**, *6*, 338. [CrossRef]
27. Dhara, A.; Hodes, G.; Sarkar, S.K. Two stage chemical bath deposition of MoO_3 nanorod films. *RSC Adv.* **2014**, *4*, 53694–53700. [CrossRef]
28. Konnert, J.H.; Appleman, D.E. The crystal structure of low tridymite. *Acta Crystallogr.* **1978**, *B34*, 13. [CrossRef]
29. Tridymite, R. Available online: https://rruff-2.Geo.Arizona.Edu/tridymite/r090042 (accessed on 10 February 2020).
30. Edy, R.; Huang, G.; Zhao, Y.; Guo, Y.; Zhang, J.; Mei, Y.; Shi, J. Influence of reactive surface groups on the deposition of oxides thin film by atomic layer deposition. *Surf. Coat. Technol.* **2017**, *329*, 149–154. [CrossRef]
31. Kamoun, O.; Boukhachem, A.; Mrabet, C.; Yumak, A.; Petkova, P.; Boubaker, K.; Amlouk, M. Effect of europium content on physical properties of In_2O_3 thin films for sensitivity and optoelectronic applications. *Bull. Mater. Sci.* **2016**, *39*, 777–788. [CrossRef]
32. Li, X.-L.; Liu, J.-F.; Li, Y.-D. Low-temperature synthesis of large-scale single-crystal molybdenum trioxide (MoO_3) nanobelts. *Appl. Phys. Lett.* **2002**, *81*, 4832–4834. [CrossRef]
33. Senthilkumar, R.; Anandhababu, G.; Mahalingam, T.; Ravi, G. Photoelectrochemical study of MoO_3 assorted morphology films formed by thermal evaporation. *J. Energy Chem.* **2016**, *25*, 798–804. [CrossRef]

34. Ramana, C.V.; Atuchin, V.V.; Troitskaia, I.B.; Gromilov, S.A.; Kostrovsky, V.G.; Saupe, G.B. Low-temperature synthesis of morphology controlled metastable hexagonal molybdenum trioxide (MoO_3). *Solid State Commun.* **2009**, *149*, 6–9. [CrossRef]
35. Joni, I.M.; Nulhakim, L.; Vanitha, M.; Panatarani, C. Characteristics of crystalline silica (SiO_2) particles prepared by simple solution method using sodium silicate (Na_2SiO_3) precursor. *J. Phys. Conf. Ser.* **2018**, *1080*, 012006. [CrossRef]
36. Wongkrua, P.; Thongtem, T.; Thongtem, S. Synthesis of h- and α-MoO_3 by refluxing and calcination combination: Phase and morphology transformation, photocatalysis, and photosensitization. *J. Nanomater.* **2013**, *2013*, 702679. [CrossRef]
37. Mimouni, R.; Askri, B.; Larbi, T.; Amlouk, M.; Meftah, A. Photocatalytic degradation and photo-generated hydrophilicity of methylene blue over ZnO/$ZnCr_2O_4$ nanocomposite under stimulated UV light irradiation. *Inorg. Chem. Commun.* **2020**, *115*, 107889. [CrossRef]
38. Chen, Y.; Lu, C.; Xu, L.; Ma, Y.; Hou, W.; Zhu, J.-J. Single-crystalline orthorhombic molybdenum oxide nanobelts: Synthesis and photocatalytic properties. *CrystEngComm* **2010**, *12*, 3740–3747. [CrossRef]
39. Ku, Y.; Huang, Y.-H.; Chou, Y.-C. Preparation and characterization of ZnO/TiO_2 for the photocatalytic reduction of Cr(vi) in aqueous solution. *J. Mol. Catal. A Chem.* **2011**, *342–343*, 18–22. [CrossRef]
40. Song, L.X.; Xia, J.; Dang, Z.; Yang, J.; Wang, L.B.; Chen, J. Formation, structure and physical properties of a series of α-MoO_3 nanocrystals: From 3d to 1d and 2d. *CrystEngComm* **2012**, *14*, 2675–2682. [CrossRef]
41. Vijay, M.; Selvarajan, V.; Sreekumar, K.P.; Yu, J.; Liu, S.; Ananthapadmanabhan, P.V. Characterization and visible light photocatalytic properties of nanocrystalline TiO_2 synthesized by reactive plasma processing. *Sol. Energy Mater. Sol. Cells* **2009**, *93*, 1540–1549. [CrossRef]
42. Mageshwari, K.; Mali, S.S.; Sathyamoorthy, R.; Patil, P.S. Template-free synthesis of mgo nanoparticles for effective photocatalytic applications. *Powder Technol.* **2013**, *249*, 456–462. [CrossRef]
43. Tariq, N.; Fatima, R.; Zulfiqar, S.; Rahman, A.; Warsi, M.F.; Shakir, I. Synthesis and characterization of MoO_3/$CoFe_2O_4$ nanocomposite for photocatalytic applications. *Ceram. Int.* **2020**, *46*, 21596–21603. [CrossRef]
44. Anjaneyulu, R.B.; Mohan, B.S.; Naidu, G.P.; Muralikrishna, R. Visible light enhanced photocatalytic degradation of methylene blue by ternary nanocomposite, MoO_3/Fe_2O_3/rGO. *J. Asian Ceram. Soc.* **2018**, *6*, 183–195. [CrossRef]
45. Balu, S.; Uma, K.; Pan, G.-T.; Yang, T.C.-K.; Ramaraj, S.K. Degradation of methylene blue dye in the presence of visible light using SiO_2@α-Fe_2O_3 nanocomposites deposited on SnS_2 flowers. *Materials* **2018**, *11*, 1030. [CrossRef]
46. Mishra, D.D.; Tan, G. Visible photocatalytic degradation of methylene blue on magnetic $SrFe_{12}O_{19}$. *J. Phys. Chem. Solids* **2018**, *123*, 157–161. [CrossRef]
47. Xu, Y.-H.; Liang, D.-H.; Liu, M.-L.; Liu, D.-Z. Preparation and characterization of Cu_2O–TiO_2: Efficient photocatalytic degradation of methylene blue. *Mater. Res. Bull.* **2008**, *43*, 3474–3482. [CrossRef]